

# Time-Resolved Volumetric Separation Measurement in a Towing Tank Using the TSI-V3V Measurement System

E. Wolf<sup>1</sup>, C. Kähler<sup>1</sup>  
D. Troolin<sup>2</sup>, C. Kykal<sup>3</sup> and W. Lai<sup>2</sup>

<sup>1</sup>Institute for Fluid Mechanics and Aerodynamics, Bundeswehr University Munich  
Werner-Heisenberg-Weg 39, 85577 Neubiberg, GERMANY  
christian.kaehler@unibw.de

<sup>2</sup>TSI Incorporated, 500 Cardigan Road, Shoreview, MN 55126, USA  
dan.troolin@tsi.com, wing.lai@tsi.com

<sup>3</sup>TSI GmbH, Neuköllner Strasse 4, 52068 Aachen, GERMANY  
carsten.kykal@tsi.com

## ABSTRACT

The present paper presents time-resolved volumetric measurements on the SD7003 airfoil, performed in a water towing tank at a Reynolds number of 60,000 and a 4° angle of attack. Under these conditions a mid-chord and stable laminar separation bubble (LSB) occurs on the suction side of the airfoil. As former investigations by means of Particle Image Velocimetry (PIV), the present study focuses on the unsteady 3D topology of the bubble. For this reason the time-resolved Volumetric 3-Component Velocimetry (V3V) technique was applied, which is highly capable of capturing a truly volumetric velocity distribution instantaneously in a nearly cubic volume. Furthermore, towing the airfoil through the resting fluid leads to a negligible turbulence level, and it is possible to observe the flow from the leading edge to the far wake of the airfoil, along with the interaction between the starting- and tip-vortex with its effect on the separation behavior. Thereby, the influence of the tip-vortex was systematically studied by changing the gap between the tank's bottom and the airfoil's tip. As a result, the three-dimensional coherent vortex structures shed near the reattachment region were detected. It is shown that the vortices possess a limited span-wise width and are arranged in a regular pattern in span- and stream-wise direction. Downstream of the bubble, the structures decay, whereas their relative positions among each other do not alter significantly.

## 1. INTRODUCTION

To this day, the interest in unmanned air vehicles (UAVs) has continuously increased. Typically working at low Reynolds numbers, UAVs possess a high tendency to cause flow separation. But especially, the presence or bursting of a LSB causes a serious change of flight dynamics. The phenomenology of the LSB has been studied in the literature for decades. This is mainly due to the fact, that the important fluid mechanical effects, such as separation, transition and turbulence, can be examined simultaneously on a small scale. Gaster [1] and Horton [2] developed a model of a two-

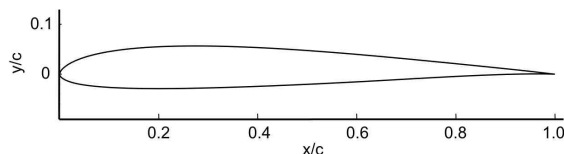


Fig. 1. The SD7003 airfoil

dimensional steady LSB. With it, they investigated the dependency on the adverse pressure gradient as well as on the Reynolds number. However, both the unsteady and three-dimensional properties have been a matter of numerous investigations. Using the Time-Resolved-PIV technique, Hain and Kähler [3] discussed the Tollmien-Schlichting instability (T-S)-waves and its relationship with the vertical oscillation of the LSB formed on the suction side of the SD7003 airfoil (see figure 1). Furthermore, Zhang et al. [4] mapped Kelvin-Helmholtz (K-H) vortex structures, whose instabilities are traceably responsible for transition in an LSB. They also examined  $\lambda$ -shape vortices. Whereas three-dimensional, unsteady and complex phenomena are investigated, there is a need for three-component velocimetry techniques, such as Stereo-Scanning PIV approved by Hori & Sakakibara [5] or Tomographic PIV by Elsinga et al. [6]. Also applying the Stereo-Scanning PIV, Burgmann et al. [7] focused on the phenomenology of the shed vortices. He detected the presence of C-shape vortices, separating periodically from the main recirculation region and moving further downstream. But a more detailed analysis of these matters is essential to improve the fundamental fluid mechanical understanding and the existing CFD-methods. The temporal and spatial development of the coherent vortex-structures is strongly unsteady and should be investigated by time-resolved techniques likewise in an instantaneous volumetric way. In regards to that, the V3V technique, which was applied in the present study, is very suitable.

## 2. EXPERIMENTAL SETUP

### 2.1 V3V technique

The Volumetric 3-Component Velocimetry (V3V) technique was developed by TSI. The system's core consists of three 4 Mega-Pixel CCD cameras arranged in a triangular configuration. The depth information can be obtained by detecting the position of individual particle images on the three different recordings after a proper calibration. In contrast to Scanning-PIV, the 3D-flow field can be captured simultaneously with the V3V technique, with the added benefit of a much larger measurement volume. The system is characterized by its very compact nature. Furthermore, it allows recording time sequences of several minutes and the fast evaluation of the data makes it very attractive (only a few minutes per volumetric vector field). Recent studies by Troolin & Longmire [8] and Hill et al. [9] provide a detailed description how the V3V system operates.

For the present experiment, a frequency-doubled New Wave YAG200-NWL dual-head pulsed Nd:YAG laser with 200 mJ at 15 Hz was applied to illuminate the 50  $\mu\text{m}$  particles. The laser beam was shaped into a cone using appropriate lenses. The measurement volume was up to  $120 \times 120 \times 100 \text{ mm}^3$  in the present experiments.

### 2.2 Test facility

As a test facility, a water towing tank of  $8.0^L \times 0.9^W \times 1.0^H \text{ m}^3$  was used. The towing device consists of a rail car running upon the tank, which is controlled precisely using a computer, where acceleration and speed are continuously adjustable in a range of 0 to 1.3 m/s. Due to these facts, the complete flow from the leading edge to the wake is observable. However, with respect to the bias of two-dimensional flow and separation behavior, the measurement volume at the span's half point should not be altered by span-wise velocities arising from the tip-vortex' influence. Hence, the gap between the airfoil's tip and the bottom of the tank had to be minimized. For this reason the unevenness of the tank's bottom was gauged in the run-up to the measurements. Thereby the  $X$ -values were charted as soon as the bottom height ( $Z$ ) had changed about a full millimeter. The resulting curve is shown in figure 2, where  $Z = 0$  represents the region of highest depth. Through the exaggerated axial ratio (approx. 400 : 1), the unevenness is pointed out clearly. The vertical position of the airfoil was adjustable using a special adapter, which is presented in the following.

### 2.2 Construction

The constructive work included the creation of both an airfoil and a proper adapter. With respect to the speed range of the towing device, the chord length of the airfoil was set to 300 mm and the width to 500 mm. It was manufactured out of massive Perspex and afterwards carefully polished to avoid any surface reflections. The fully transparent nature of the airfoil made it possible to measure the flow field on the upper and lower side of the airfoil simultaneously by using the V3V technique. Thereby, a concave form was milled on both sides with a view, to stabilize the material for the cutting (especially regarding the 0.4 mm thin trailing edge) and the polishing. The airfoil was fixed on an aluminum plate and pinned with a shaft at  $x/c = 0.25$ , where the expected aerodynamic moments are small. A frustum, serving as an indicator, was connected at the other end of the shaft very accurately to guarantee a true transmission of the angle of attack. The angle adjustment happened by means of a rotary table (see figure 3), usually used for optic applications. Thus the angle of attack

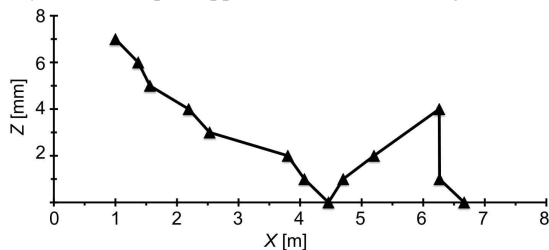


Fig. 2. Unevenness of the towing tank's bottom



Fig. 3. Rotary table for angle adjustment



Fig. 4. 3-clamp system

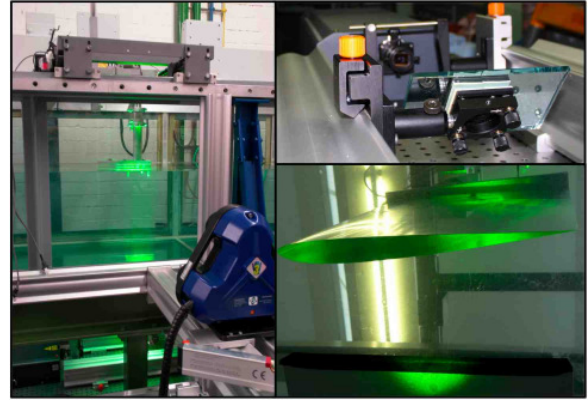


Fig. 5. Test set-up with the V3V system

was continuously variable from  $360^\circ$ . A simple and precise height adjustment was realized by a three-clamp system (see figure 4). Using two obstructed clamps and one free clamp, the vertical and angle adjustments can be isolated from each other. With this arrangement, the adapter is completely manageable by one person. The locus of test section was defined considering the unevenness of the tank's bottom, the model size and the performance of the towing device. The laser was installed underneath the test section, whose light cone was turned upwards (see figure 5). Additionally, some light-impermeable material was fixed under the channel to form the laser cone into a discrete and straight volume. Furthermore, the V3V camera was arranged at right angles with the section walls and in proper height (centre of measurement volume at the span's half point). The adapter and the airfoil were hung up at the rail car's designated holding fixture so that the airfoil could be lowered to reduce the gap to less than 2 mm in the test section.

## 3. RESULTS

The measurements were performed at  $\alpha = 4^\circ$  and  $Re = 60,000$ , which corresponds with a free stream velocity of  $u_\infty = 0.2 \text{ m/s}$ . As a reference, the angle of attack  $\alpha = 8^\circ$  was investigated. For particle tracking, a 50  $\mu\text{m}$  polyamide (PA) seeding was used. Previous analyses have shown that these particles do not clump up. Due to the total filling volume of the tank, frequent added seeding was necessary during the experiments. Note that the addition of the PA-tracers took a little time to homogenize. All visualizations were produced with TECPLOT.

### 3.1 Disturbed airfoil flow

In order to examine the three-dimensional coherent vortex structures the free-stream should be necessarily two-dimensional and uninfluenced. For this reason the two major influences such as starting-vortex and tip-vortex were examined in the beginning. The airfoil was lifted about 10 cm from the bottom, just as the measurement volume (V3V camera) was positioned properly. During evaluation, the towing speed was added to the velocity vector field. Furthermore, because of a higher lift coefficient, the investigations for an  $8^\circ$  angle of attack were found to be good at presenting the tip- and starting-vortex.

#### 3.1.1 Tip-vortex

First of all, the unsteady flow was examined, which has a tip-vortex as a result. Its temporal-spatial development is shown in figure 6. For this purpose, iso-surfaces of a negative second Eigen value  $\lambda_2$  were plotted and contoured with the

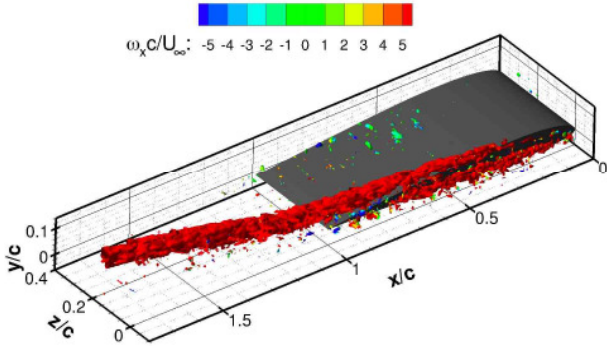


**Fig. 6.** Development of a tip-vortex for  $\alpha = 8^\circ$ ;  $\lambda_2$ -iso-surfaces flooded with normalized stream-wise vorticity

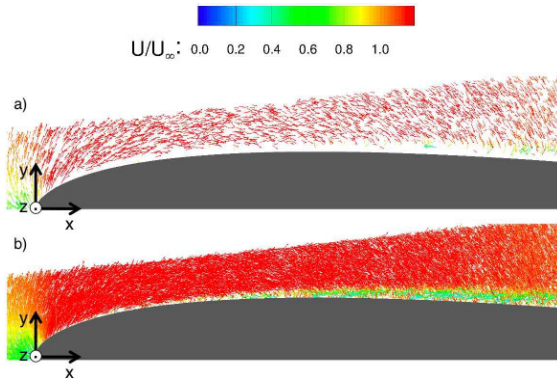


**Fig. 7.** Distribution of particle vectors in dependency of the tip distance; vectors flooded with  $U / U_\infty$ -magnitude

normalized wall-parallel swirling strength. The tip-edge is located at  $z = 0$ . For the evaluation process, the vector fields recorded at different times were shifted according to  $\Delta x = u_\infty / f$ , where  $f$  is the camera frame rate (7.25 Hz). Because of this, overlapping structures might be interpreted as new coherent ones. Nevertheless, one recognizes the tip-vortex' history as expected. Additionally, the wall-normal plane near the leading edge is pictured in figure 7. The instantaneously recorded vectors are flooded with their normalized stream-wise velocity magnitude. Whereas in figure 7 a) only particle vectors, which are far from the tip ( $z \geq 0.3c$ ), were indicated, in figure 7 b) all vectors were depicted. All in all, its swirling motion causes a strong boundary layer mixing nearby.

### 3.1.2 Starting-vortex

Figure 8 shows the starting-vortex interacting with the tip-vortex, 0.69 s after the airfoil has started. In the left image, the planes are contoured by the instant particle velocity distribution ( $u_\infty$  was not yet added). Additionally, particle vectors indicate the real 3D-flow behavior. Tip- and starting-vortices were detected with the aid of the  $\lambda_2$ -criterion and

flooded by the span-wise vorticity. In the right picture, apart from identical velocity distribution, two iso-surfaces of opposing magnitudes are depicted. Further streamlines were inserted to demonstrate the helical character of the tip-vortex. Because of friction along the airfoil's tip, the flow is carried away. Coincidentally, the swirling motion stabilizes this effect and the influence of both the tip-vortex and the starting-vortex is locally limited.

### 3.2 Undisturbed airfoil flow

Having the airfoil lowered and the gap between the airfoil's tip and the bottom of the tank reduced below 2 mm, the incident flow near the span's mid-point is two-dimensional. As a consequence, three-dimensional coherent vortex structures can be distinguished.

#### 3.2.1 Vortex shedding

The instant stream-wise velocity distribution is shown in figure 9. Due to the fact that the boundary layer was not resolved, the particle vectors were plotted to verify the credibility of the data. This is necessary because every vacancy is replaced by an interpolated vector. However, downstream of  $x/c = 0.7$ , there are several areas of a decreased stream-wise velocity magnitude ( $u / u_\infty = 0.5$ ). With the aid of  $\lambda_2$ -iso-surfaces, the corresponding vortices could be located as well. As further measurements confirmed, these vortices shed more-or-less in a chessboard pattern. They have an approximate size of  $0.04^x \times 0.04^y \times 0.06^z c^3$ . Furthermore the vortices are flooded by contours of the normalized swirling strength. Whereas the normalized span-wise vorticity  $\omega_z c / u_\infty$  is uniformly negative, both  $\omega_x c / u_\infty$  and  $\omega_y c / u_\infty$  are distributed asymmetrically on the edge regions of the vortices. This underlines the three-dimensional character of these structures and stands in interdependency of a regular distribution of sources and sinks. However, because of the lack of seeding particles in the boundary layer and the regular vector grid size of 2 mm, the topology of these vortices cannot be examined with more precision.

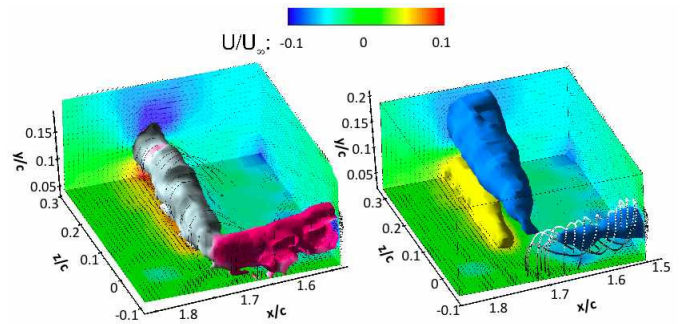


**Fig. 8.** Starting-vortex (white) and tip-vortex (pink);  $\lambda_2$ -iso-surfaces (left) and  $U / U_\infty$ -iso-surfaces (right)

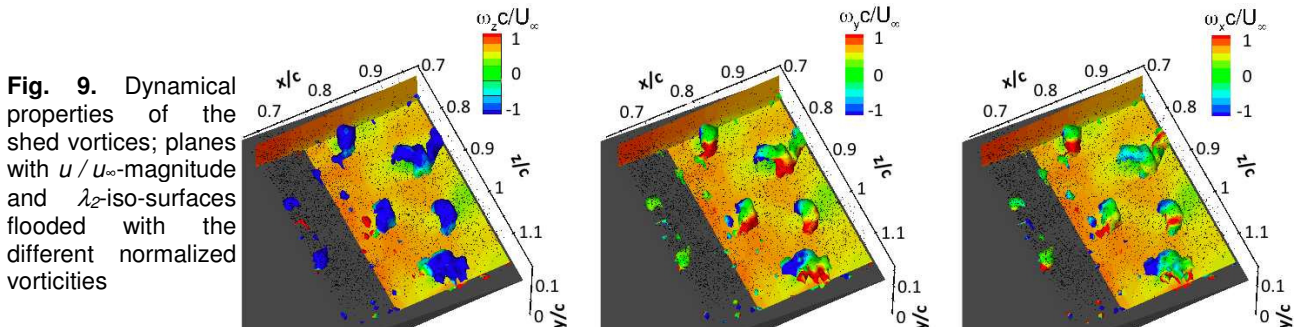


**Fig. 9.** Dynamical properties of the shed vortices; planes with  $U / U_\infty$ -magnitude and  $\lambda_2$ -iso-surfaces flooded with the different normalized vorticities

### 3.2.2 Vortex evolution

Figure 10 shows the temporal-spatial development of the known group of vortices. For this purpose, the vortex cores were identified with  $\lambda_2$ -iso-surfaces and flooded by their  $y$ -position to clear their 3D-position. Furthermore, asymmetric iso-surfaces of the normalized wall-normal vorticity were added to distinguish between individual vortices. At  $t_0$ , the structures A to E are located in the same plane. Thus, vortices A, C and E are equally spaced at a distance of  $0.15 c$  from each other along a fictitious span-wise line. Having a similar distance among each other, the vortices B and D are displaced approximately  $0.1 c$  in the downstream direction, and diagonally shifted. Until  $t_0 + 3 \Delta t$  ( $\Delta t = 0.138$  s), all vortices have reached their maximum size and moved slightly downstream. Furthermore, a new larger structure F has slid in the range. In the meantime, C approached D, but until  $t = t_0 + 7 \Delta t$ , it descended out of the measurement volume in the  $y$ -direction. During this process, the resting vortices moved downstream, without altering their positions among each other in the surface-parallel plane. Regarding the vortices' grayscale, F extends further in the  $y$ -position. Considering the convection velocity and the vortices' spacing, one can estimate the shedding frequency. Comparing the constellation of the first two frames ( $t_0$  and  $t_0 + \Delta t$ ), vortex A, for instance, has moved  $0.05 c$  (15 mm). Having a camera frame rate of  $f = 7.25$  Hz, the convection velocity is  $u_c = 0.11$  m/s, which corresponds with a frequency of 7.3 Hz for the vortex shedding. Afterwards the large-scale structure F, frequently detected during the experiments, was investigated in detail. In figure 11 the  $\lambda_2$ -iso-surface was flooded with the normalized span-wise swirling strength and the particle vectors were inserted. Here the  $y$ - and  $z$ -extensions (approx.  $0.12 c$ ) are obvious. The volume below  $y = 0.05 c$  contains almost no particle vectors, as this volume was blocked from laser illumination. Hence, iso-surfaces are not shown below this level. Consequently, no statement about this vortex' topology can be given, except that it has a half-ring shape in the valid range, as observed in [4].

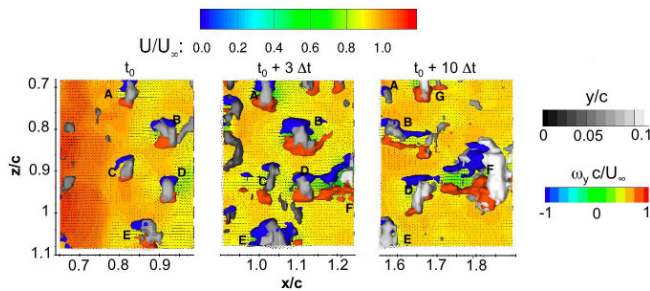


**Fig. 10.** Development of the shed vortices;  $u/u_\infty$ -planes,  $\lambda_2$ -iso-surfaces flooded with  $y$ -position and  $\omega_y c / u_\infty$ -iso-surfaces

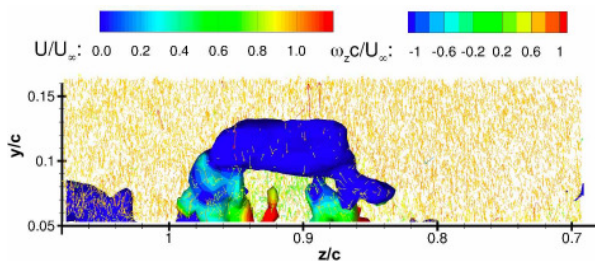


**Fig. 11.** Large-scale structure F; particle vectors flooded with  $u/u_\infty$ -magnitude and  $\lambda_2$ -iso-surfaces flooded with the normalized span-wise vorticity magnitude

## 4. CONCLUSIONS

The objective of this study was the quantitative investigation of unsteady coherent vortex structures arising from the point of reattachment of an LSB using the innovative V3V technique. The experiments were performed in a water towing tank at  $Re = 60,000$  and  $\alpha = 4^\circ$ . First of all, the effect of the tip- and starting-vortex on the two-dimensionality of the flow was examined. Consequently, the influences were minimized by the test set-up where a two-dimensional incident flow was investigated. Thereby, at 70 % of the chord, a group of vortices was detected, having a regular order (chessboard) and corresponding with a regular distribution of sinks and sources. The shed vortices' further development was time-resolved. Additionally, a large-scale structure, which extended into the illuminated volume, was detected but neither the boundary layer nor the detailed dynamics of its structure that extended outside of the illuminated volume were resolved. The V3V system is very valid for the fast and three-dimensional quantitative observation of a big volume as it was necessary for the present study.

## ACKNOWLEDGMENTS

The authors like to thank Prof. Münch and Mr. Banachowicz from the Bundeswehr University Munich for providing the test facility and their technical support.

## REFERENCES

- [1] Gaster M. (1966) The Structure and Behaviour of Laminar Separation Bubbles. *AGARD CP-4*, 813-854.
- [2] Horton H. (1968) Laminar Separation Bubbles in Two and Three Dimensional Incompressible Flow. *Ph.D. Thesis*, Department of Aeronautical Engineering, Queen Mary College / University of London.
- [3] Hain R. & Kähler C. (2005) Advanced Evaluation of Time-Resolved PIV Image Sequences. *6<sup>th</sup> International Symposium on Particle Image Velocimetry*, Pasadena, 21-23 September.
- [4] Zhang W., Hain R. & Kähler C. (2008) Scanning PIV Investigation of the Laminar Separation Bubble on a SD7003 Airfoil. *Experiments in Fluids*, **45**, 725-743.
- [5] Hori T., Sakakibara J. (2004) High-Speed Scanning Stereoscopic PIV for 3D Vorticity Measurement in Liquids. *Measurements Science and Technology*, **15**, 1067-1078.
- [6] Elsinga G., Scarano F., Wieneke B. & Oudheusden B. van (2006) Tomographic Particle Image Velocimetry. *Experiments in Fluids*, **41**, 933-947.
- [7] Burgmann S., Dannemann J. & Schröder W. (2007) Time-Resolved and Volumetric PIV Measurements of a Transitional Separation Bubble on an SD7003 Airfoil. *Experiments in Fluids*, **44**, 609-622.
- [8] Troolin D. & Longmire E. (2008) Volumetric 3-Component Velocity Measurements of Vortex Rings from Inclined Exits. *14<sup>th</sup> International Symposium on Applications of Laser Techniques to Fluid Mechanics*, Lisbon, Portugal, 07-10 July.
- [9] Hill D., Troolin D., Walters G., Lai W. & Sharp K. (2008) Volumetric 3-Component Velocimetry Measurements of the Turbulent Flow in Stirred Tank Reactors. *14<sup>th</sup> International Symp. on Applications of Laser Techniques to Fluid Mechanics*, Lisbon, Portugal, 07-10 July.